Water Resources Research®

RESEARCH ARTICLE
10.1029/2024WR039321

Key Points:

- Satellite soil moisture and terrestrial water storage illustrate the propagation and recovery of water deficits in the sub-surface
- Daily water storage data from satellite gravimetry are valuable for quantifying drying and re-wetting rates
- The results reveal the cascading effect of drought dynamics from the surface through the root zone to the entire sub-surface storage

Supporting Information:

Supporting Information may be found in the online version of this article.

Correspondence to:

D. Blank,
daniel.blank@hcu-hamburg.de

Citation:

Blank, D., Eicker, A., Reager, J. T., & Güntner, A. (2025). Revisiting sub-surface drought cascades with daily satellite observations of soil moisture and terrestrial water storage. *Water Resources Research*, *61*, e2024WR039321. https://doi.org/10.1029/2024WR039321

Received 30 OCT 2024
Accepted 25 JUL 2025

Author Contributions:

Conceptualization: Daniel Blank, Annette Eicker, John T. Reager, Andreas Güntner
Formal analysis: Daniel Blank
Methodology: Daniel Blank, Annette Eicker
Project administration: Annette Eicker
Software: Daniel Blank
Supervision: Annette Eicker
Visualization: Daniel Blank
Writing – original draft: Daniel Blank, Annette Eicker, Andreas Güntner
Writing – review & editing: Daniel Blank, Annette Eicker, John T. Reager, Andreas Güntner

© 2025. The Author(s).
This is an open access article under the terms of the Creative Commons Attribution License, which permits use, distribution and reproduction in any medium, provided the original work is properly cited.

Revisiting Sub-Surface Drought Cascades With Daily Satellite Observations of Soil Moisture and Terrestrial Water Storage

Daniel Blank[1], **Annette Eicker**[1], **John T. Reager**[2], **and Andreas Güntner**[3,4]

[1]HafenCity University Hamburg, Hamburg, Germany, [2]Jet Propulsion Laboratory, California Institute of Technology, Pasadena, CA, USA, [3]Helmholtz Centre Potsdam GFZ German Research Centre for Geosciences, Potsdam, Germany, [4]Institute of Environmental Sciences and Geography, University of Potsdam, Potsdam, Germany

Abstract The increasing frequency, intensity, and duration of extreme heat and drought events in a warming climate make it crucial to understand the relationship between surface and subsurface water storage dynamics during these events. Changes in water storage can be studied globally using satellite observations. Microwave remote sensing observes the upper few centimeters of the soil, while satellite gravimetry detects changes in the entire column of terrestrial water storage. We use daily data of the Gravity Recovery and Climate Experiment (GRACE) and GRACE Follow-On (GRACE-FO), satellite-based surface soil moisture data and root zone products from Soil Moisture Ocean Salinity, Soil Moisture Active Passive, and European Space Agency Climate Change Initiative on a harmonized 1° global grid to study the evolution of water storage deficits across different soil layers. The joint analysis of the three types of data provides valuable insight into the hydrological dynamics in different soil depths and subsurface water storage compartments. To identify different dynamics, we compute the rate of change from de-seasonalized water storage anomaly time series to assess how quickly the system accumulates storage deficits during drought conditions and recovers from them for different integration depths in the subsurface. The results indicate characteristic patterns of the temporal dynamics of drought recovery with fast fluctuations and short recovery times for surface soil moisture, a prolonged behavior in the root-zone, and an even slower response in the entire water column. This highlights that the cascading propagation of drought dynamics from the surface to the subsurface can be quantified by remote sensing data with daily resolution at the global scale.

1. Introduction

In a warming climate, the frequency, intensity, and duration of extreme heat and drought events are expected to increase (Seneviratne et al., 2021). Therefore, it is more important than ever to comprehend the relationship between surface and subsurface water dynamics during extreme events and their evolution. Droughts, characterized by prolonged periods of significantly low precipitation and high temperatures, pose a substantial environmental challenge with widespread consequences. In an ecosystem, the lack of sufficient water not only reduces the available water for human needs but also has major ecological effects, stressing and depleting plant and animal life. There are four different types of drought based on their length, severity, and effects: meteorological, agricultural, hydrological, and socio-economic drought (Crocetti et al., 2020; Mishra & Singh, 2010; Wilhite & Glantz, 1985). The first three types pertain to the physical aspects of the phenomenon, whereas the socio-economic drought is linked to the societal impacts. To focus on the physical aspects, a meteorological drought is defined as a prolonged lack of precipitation, an agricultural drought as a persistent insufficiency in soil moisture availability, and a hydrological drought as a continuous deficit in streamflow or groundwater storage.

All these three types of droughts are connected, and by using ground data from Illinois on precipitation, soil moisture, shallow groundwater levels, and streamflow, Changnon (1987) developed one of the first frameworks for evaluating the evolution of droughts across variables. The theoretical drought cascade originally defined in that study delineates the initiation of drought signals in the atmosphere, resulting in a meteorological drought. Afterward, these signals are delayed in sequence, affecting runoff, soil moisture, streamflow, and groundwater. An important feature that this theory suggests is that the time series of the drought signals get dampened and delayed as they move down the cascade from meteorology to subsurface variables (i.e., from precipitation to groundwater). The conceptual explanation of drought propagation and recovery has been confirmed in other research, for example, by Peters et al. (2006), who examined groundwater drought processes in the Pang catchment (United Kingdom) through simulated groundwater patterns and by Van Loon (2015), who used hydrological models to analyze droughts in four distinct types of European river basins. Closely linked to drought propagation and recovery and the role of water storage on the Earth's climate system is the concept of soil moisture memory, that is, the mechanisms with which soils preserve the information on storage anomalies over time, including its depth-dependence (Rahmati et al., 2024).

Existing studies have shown the cascading effects of droughts across larger regions and multiple events, primarily through ground observations (Bae et al., 2019; Barker et al., 2016; Bhardwaj et al., 2020; Huang et al., 2017; Oertel et al., 2018; Tijdeman et al., 2018). The integration of remote sensing data has emerged as a valuable tool for understanding large-scale drought phenomena on a global scale (AghaKouchak et al., 2015). Although studies so far have been rare, utilizing remote sensing data to analyze drought propagation and recovery across variables could be advantageous in characterizing cascading effects over large domains Farahmand et al. (2021) employ satellite observations to characterize cascade phenomena in four major United States (US) drought case studies, whereas Rossi et al. (2023) focuses on characterizing major drought events and their propagation in three Brazilian regions. Entekhabi (2023) use remote sensing data and in situ observations to study the drought cascade and its characteristics over the continental US. A feature that all of these studies have in common is that they use monthly terrestrial water storage (TWS) data from the GRACE/GRACE-FO satellite gravimetry mission to represent the hydrological drought component.

Due to the fact that any redistribution of water mass on or above the Earth's surface leads to variations of the Earth's gravity field, satellite gravimetry can relate changes in the gravitational acceleration acting on a satellite to variations in TWS on and underneath the Earth's surface but cannot distinguish between water mass changes in individual water compartments (e.g., soil moisture, snow cover, groundwater, surface water). The twin satellite mission GRACE (Tapley et al., 2004), and its successor mission GRACE-FO (Landerer et al., 2020) have been observing gravity field changes since 2002. However, the temporal resolution of standard GRACE data for 1 month is too low to record any fast water mass changes and restricts the temporal resolution of the drought propagation analysis to a monthly range. Recent developments in GRACE data processing (Kvas et al., 2019) have enabled the computation of daily gravity fields with increased accuracy. Such daily gravity data were successfully used in various studies (Bergmann & Dobslaw, 2012; Bonin & Chambers, 2011; Eicker et al., 2020; Gouweleeuw et al., 2018; Xiong et al., 2022). Blank et al. (2023) have shown that TWS signal content is related to soil moisture variations seen in remote-sensing soil moisture products, albeit with temporal delay. They used cross-correlation analysis for the determination of time shifts between time series from which only the linear trend was removed. It was the first study in which GRACE data with a higher than monthly resolution were compared with soil moisture data.

Using daily data from TWS from GRACE/GRACE-FO appears particularly promising for a more detailed and comprehensive analysis of the dynamics of drought cascades but has not been used for this specific purpose yet. The daily resolution can capture rapid changes and short-term fluctuations in the water storage variables, offering a more comprehensive understanding of the cascading effects and enabling the identification and analysis of short-term drought events that might be overlooked when using monthly data. In addition to TWS data from GRACE, this study integrates remotely-sensed soil moisture data for an assessment of surface soil moisture (SSM) conditions that predominantly represent agricultural drought. Additionally, including root zone soil moisture (RZSM) to soil depths of up to 1 m offers insights into deeper soil layers. The main goal of this study is to use remote sensing for investigating how drought affects water storage in the subsurface across different layers, from the top layer to the root zone and finally to the whole water column of TWS, including the deeper unsaturated zone and the groundwater. By exploring these different integration depths, the study seeks to add comprehensive insights into the sub-surface components of the drought cascade, that is, how drought propagates and recovers with depth and, thus, into the overall hydrological response to prolonged water deficits. Although the physical phenomenon of drought cascades including terrestrial water storage data from satellite gravimetry has exemplarily been analyzed before (see references above), our investigation differs from these previous studies with respect to (a) the methodology, (b) the global extent of the analyses, (c) the specific soil moisture data sets, and (d) the higher observation-based temporal resolution of daily GRACE data.

The paper is structured as follows: Section 2 describes the satellite data products used for the quantification of soil moisture (SM) and total water storage (TWS). Section 3 discusses data processing and limitations of the data sets. In Section 4, the methodology and the corresponding results for calculating the recovery times of droughts are

19447973, 2025, 8, Downloaded from https://agupubs.onlinelibrary.wiley.com/doi/10.1029/2024WR039321 by Hafencity Universitaet Hamburg, Wiley Online Library on [18/02/2026]. See the Terms and Conditions (https://onlinelibrary.wiley.com/terms-and-conditions) on Wiley Online Library for rules of use; OA articles are governed by the applicable Creative Commons License

explained in detail. Starting with the calculation of seasonal anomalies from each time series, we can identify periods of storage deficit when water storage is below normal levels. The variability observed during these drought periods is then utilized to estimate the probable recovery times as a measure to characterize drought behavior. Results are first presented for an exemplary time series to illustrate the subsequent steps of the approach and afterward extended to the global scale.

2. Data Sets

2.1. GRACE and GRACE-FO Data

Daily gravity field solutions were computed from GRACE and GRACE-FO observations as part of the ITSG-Grace2018 gravity field time series (Kvas et al., 2019) in the form of spherical harmonic coefficients up to degree $n = 40$ (corresponding to a spatial resolution of 500 km) to examine rapid, short-term fluctuations in terrestrial water storage (TWS) and its anomalies. In contrast to the conventional monthly solutions, the restricted satellite ground track coverage within a single day does not support a robust global gravity field inversion. Therefore, to address this limitation, the daily gravity solutions from ITSG-Grace2018 are generated within the framework of a Kalman smoothing approach (similar to Kurtenbach et al. (2012)), which integrates statistical information on the expected evolution of the gravity field over time into its process model. As a trade-off, the daily gravity field data that result from this approach are not entirely standalone solutions. Instead, they display a certain level of correlation with neighboring time steps.

In the process of data handling, temporally high-frequency mass fluctuations attributed to tides (ocean, Earth and pole tides), along with non-tidal variations in atmospheric and oceanic mass, are removed by subtracting the output of geophysical background models from the observations (de-aliasing, Dobslaw et al. (2017)). Following this step, additional post-processing measures are taken: Geocenter motion is addressed by incorporating the degree-1 harmonic coefficients provided by Sun et al. (2016) on the basis of Swenson et al. (2008). The c_{20} coefficient is replaced with a time series derived from Satellite Laser Ranging (Cheng & Ries, 2017), and the influence of glacial isostatic adjustment (GIA) is removed by the ICE6G-D model (Peltier et al., 2017). No extra spatial filtering is needed, because the Kalman smoother effectively suppresses spatially correlated noise. Subsequent to these data processing procedures, the resulting gravity field models are presumed to predominantly represent variations in water mass both above and below the Earth's surface. The gravity field solutions can then be converted into equivalent water heights across a global geographical grid according to

$$TWS(\lambda,\vartheta) = \frac{M}{4\pi R^2 \rho_w} \sum_{n=1}^{n_{\max}} \sum_{m=-n}^{n} \frac{(2n+1)}{(1+k'_n)} c_{nm} \Upsilon(\lambda,\vartheta) \tag{1}$$

where λ and ϑ symbolize the spherical coordinates, M and R are the mass and the radius of the Earth, ρ_w is the density of water $\left(\frac{1000\text{kg}}{m^3}\right)$, k'_n denote the Load Love Numbers (Lambeck, 1988), c_{nm} are the spherical harmonic coefficients of the gravitational potential, and $\Upsilon(\lambda,\vartheta)$ are the surface spherical harmonic functions. The degree and order of the spherical harmonic functions are denoted by n and m.

While the Kalman smoother output ensures a continuous daily time series during the mission time period, we selectively excluded days with insufficient GRACE observations from our analysis. Specifically, we omitted days with observation counts falling below 10,000 observations per day, as given on the ITSG-Grace2018 product website. During these days, the daily solutions primarily rely on the Kalman filter's process model, resulting in a tendency toward an a-priori mean trend and an annual signal. The calculation of GRACE TWS data was conducted using the Gravity Recovery Object Oriented Programming System (GROOPS; Mayer-Gürr et al., 2021).

2.2. Soil Moisture Data Sets

Microwave remote sensing is a method used to detect soil moisture in the uppermost soil layer by leveraging changes in the soil's dielectric constant associated with varying water content. Active microwave sensors transmit electromagnetic pulses to the Earth and measure the backscattered energy from the Earth's surface, while passive microwave sensors capture naturally emitted radiation from the Earth's soil, represented as brightness temperature (Robinson et al., 2008). Both techniques rely on the dielectric constant of the soil, influencing observed parameters such as backscattered energy and brightness temperature, enabling the measurement of soil moisture.

19447973, 2025, 8, Downloaded from https://agupubs.onlinelibrary.wiley.com/doi/10.1029/2024WR039321 by Hafencity Universitaet Hamburg, Wiley Online Library on [18/02/2026]. See the Terms and Conditions (https://onlinelibrary.wiley.com/terms-and-conditions) on Wiley Online Library for rules of use; OA articles are governed by the applicable Creative Commons License

In this study, satellite-derived surface soil moisture products from the missions Soil Moisture Ocean Salinity (SMOS; Kerr et al. (2010)), Soil Moisture Active Passive (SMAP; Entekhabi et al., 2010), and the multi-satellite combination data product from the European Space Agency Climate Change Initiative (ESA CCI; Dorigo et al., 2017; Gruber et al., 2019; Preimesberger et al., 2021) are used, as well as root-zone soil moisture products from SMOS and SMAP. Both SMOS and SMAP provide Level 3 (L3) and Level 4 (L4) data, with L3 referring to original satellite observations acquired over a 24-hr period given as a multi-orbit global map of retrieved soil moisture, and L4 relating to post-processed data products. The way of post-processing differs among the two satellite missions. The study uses an early morning overpass for L3 satellite soil moisture products, reducing temperature differences between soil surface and vegetation canopy, and reducing thermal differences within a pixel, resulting in reduced errors and improved reliability (Entekhabi et al., 2014; Lei et al., 2015; Owe et al., 2008).

ESA's SMOS satellite mission, launched in 2009, is used to observe soil moisture using an L-band radiometer. Here we use the daily L3 surface soil moisture (SSM) data and the L4 root zone soil moisture data from the Centre Aval de Traitement des Données SMOS (CATDS). The data is provided in a global grid with a spatial resolution of 25 km × 25 km (CATDS, 2022a, 2022b). The CATDS L4 root zone soil moisture (RZSM) product is generated by propagating the L3 surface soil moisture data set (representing the uppermost 0–5 cm of the soil) into the underlying soil down to a depth of 1 m by using an exponential filter, based on a modified formulation of a recursive exponential filter while considering soil properties and an optional implementation of transpiration (Al Bitar & Mahmoodi, 2020). In this way, the SMOS L4 RZSM data set used in this study represents the water storage within an integration depth of 1 m.

NASA launched the SMAP satellite in January 2015 to observe surface soil moisture with an L-band active radar and passive radiometer. In this study, L3 and L4 products from SMAP are used. The daily L3 data (v9.0; O'Neill et al., 2023) contain all surface soil moisture retrievals for an entire day mapped to a global grid with a spatial resolution of 36 km. The L4 (surface and root zone soil moisture, v7.0; Reichle et al., 2022) products are derived by assimilating SMAP surface brightness temperature observations into the Goddard Earth Observing Model System (GEOS-5, v5) catchment land surface model, which gives estimates for the surface soil moisture as well as the root zone, provided with a temporal resolution of 3 hr and a 9 km spatial resolution. Similar to the SMOS products, the integration depth of SMAP L3 and L4 SSM data is 0–5 cm, while the L4 RZSM product represents a soil depth of 1 m.

The ESA CCI surface soil moisture data set is provided as part of ESA's Climate Change Initiative, based on harmonizing and merging soil moisture retrievals from multiple satellite missions into a combined daily product. The combined active and passive surface soil moisture product (v8.1; Dorigo et al., 2023) is selected for analysis in this study, providing daily surface soil moisture observations (0–5 cm depth) with a spatial resolution of 0.25° and is available from the ESA data archive. It should be noted that tropical rainforest areas are completely masked out because of the strong signal scattering in the microwave observations caused by vegetation (Ulaby & Long, 2014).

It is important to note that both the L3 and L4 data are not purely based on satellite observations. The L3 soil moisture products from SMAP and SMOS are directly derived from the satellite data but are influenced by ancillary data that constrain the soil moisture retrieval process, for example, vegetation indices or land surface temperature. In contrast, the L4 soil moisture product from SMAP is generated through a data assimilation framework that integrates satellite soil moisture observations into a land surface model in combination with precipitation and other climate forcing variables. Therefore, the SMAP L4 product largely depends on the model and its input data.

3. Data Pre-Processing and Limitations

3.1. Data Harmonization

In this study, the analysis is carried out on a global grid cell level, therefore, all data sets are harmonized to the same $1^\circ \times 1^\circ$ geographical grid. The various soil moisture data sets, which have finer native resolutions, were downsampled using a first-order conservative remapping algorithm that preserves integrated quantities such as mass or volume. For the GRACE data it should be noted that the actual spatial resolution is even lower than 1° as the data are derived from a spherical harmonic representation that is truncated at degree and order $n = 40$ and

19447973, 2025, 8, Downloaded from https://agupubs.onlinelibrary.wiley.com/doi/10.1029/2024WR039321 by Hafencity Universitaet Hamburg, Wiley Online Library on [18/02/2026]. See the Terms and Conditions (https://onlinelibrary.wiley.com/terms-and-conditions) on Wiley Online Library for rules of use; OA articles are governed by the applicable Creative Commons License

19447973, 2025, 8, Downloaded from https://agupubs.onlinelibrary.wiley.com/doi/10.1029/2024WR039321 by Hafencity Universitaet Hamburg, Wiley Online Library on [18/02/2026]. See the Terms and Conditions (https://onlinelibrary.wiley.com/terms-and-conditions) on Wiley Online Library for rules of use; OA articles are governed by the applicable Creative Commons License

exhibits spatial dependencies between the grid cells up to a range of about 500 km for daily data (Kvas et al., 2019). Thus, the $1° \times 1°$ resolution used here represents a compromise between the higher resolution of the soil moisture products and the lower resolution of GRACE. To evaluate the potential impact of the spatial resolution, we transformed the soil moisture products into the same spherical harmonics representation and truncation as the GRACE data to mimic their resolution before re-gridding to $1° \times 1°$. The effect on the results is discussed in Section 4.4.

For a reasonable temporal overlap of all data sets, we used the time period from April 2015 (start of the SMAP mission) to December 2022 for our study, excluding the time span between the end of the mission GRACE (August 2017) and the start of the successor mission GRACE-FO (July 2018). The SMOS and SMAP missions have a maximum revisiting time of 3 days, resulting in temporal gaps in the SMOS, SMAP, and ESA CCI data. For gap filling, linear interpolation is applied, and a 3-day moving average is calculated afterward to reduce noise. Linear interpolation was only carried out for gaps lasting up to a maximum of 3 days, while gaps exceeding this duration remain unfilled, persist in the time series and were not considered for further analyses. Although this method guarantees data set continuity, the smoothing effect of the linear interpolation may cause a minor delay in representing quick changes, especially during recovery phases. Further details on the effect of the linear interpolation on the results is provided in Section 4.4. Periods with data gaps in the TWS data set (see Section 2.1) were excluded from the analyses.

3.2. De-Seasonalized and Standardized Signal

In this study, droughts are considered as periods with a water storage deficit relative to the regular climatological conditions. Therefore, residuals were computed by removing the mean, the trend, and seasonal cycle from the time series by best fitting the following equation to each soil moisture or TWS time series:

$$f(t) = a + b \cdot t + c \cdot \cos(\omega t) + d \cdot \sin(\omega t) + e \cdot \cos(2\omega t) + f \cdot \sin(2\omega t) \tag{2}$$

with parameters for the mean (a), linear trend (b), and annual and semi-annual cycles (c, d, e, f).

After removing the mean, trend and annual signal from the complete signal, a de-seasonalized signal, denoted as $D_{y,d}$ at any year y and day d, remains. Given the different units of the observations (volumetric soil moisture and equivalent water heights) and the varying integration depths of water content (SSM: 0–5 cm, RZSM: 0–1 m, TWS: all storage compartments, no depth limit), the de-seasonalized signal is standardized by dividing it by its standard deviation, resulting in the unit-less z-score time series $\mathrm{SD}_{y,d}$.

$$\mathrm{SD}_{y,d} = \frac{D_{y,d}}{\sigma_d} \tag{3}$$

The degree of correlation (generally higher for root-zone products) and the percentage value of signal sign agreements (at least above 50% for most grid cells across all soil moisture products) between the standardized signals from GRACE and the soil moisture products are presented globally in the Figures S1–S4 in Supporting Information S1.

The baseline statistics (mean, trend, and seasonal cycle) were computed using the maximum length of the overlapping observational time span available for all data sets, covering the period from 2015 to 2022. The limited length of the data record is a known constraint in satellite-based analysis. While this duration allows for the identification of relative anomalies within the observed window, it does not represent long-term climatological conditions in the conventional sense (i.e., multi-decadal climate normals). Therefore, the derived anomalies should be interpreted as deviations from the average conditions prevailing during this specific observational period, rather than as deviations from the long-term climatology.

One limitation of the de-trending approach is the potential removal of long-term groundwater storage changes which can play an important role in the persistence of hydrological droughts in the deeper sub-surface. Previous studies have demonstrated that groundwater variability operates on decadal to multi-decadal timescales and is modulated by hydrogeological and topographic factors (Barros et al., 2017; Fan, 2015). This is a recognized limitation when using relatively short time series as in our study, and it should be considered when interpreting the results.

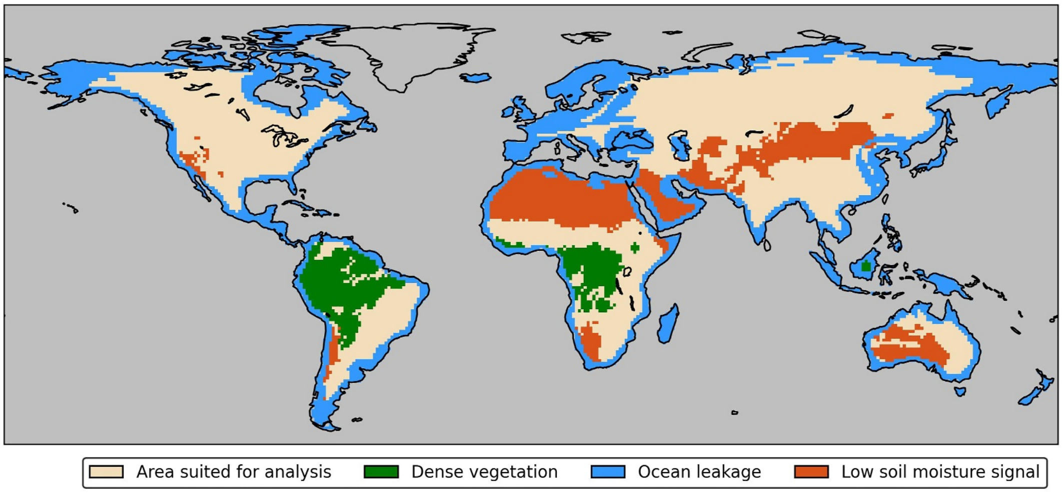

Figure 1. Spatial masks applied to exclude regions low soil moisture variability (brown), dense vegetation (green) and ocean leakage (blue) from the analysis; other areas (beige) are considered to be suited for analysis.

3.3. Spatial Limitations and Masking

The land cover type has an impact on the ability to observe soil moisture by microwave remote sensing techniques. Therefore, we apply spatial masking to exclude adversely affected regions from the analysis, see Figure 1. In densely vegetated areas, such as tropical rain forests, the vegetation has a significant impact on passive or active microwave signals (Owe et al., 2001; Ulaby & Long, 2014). While the ESA CCI data set mask out observations in rain forest regions, the other products include these regions in their data sets. For consistency in our analysis, we mask out these regions. In deserts, the soil moisture signal may be unreliable due to low variability in water content in the upper soil layers (Dorigo et al., 2010). Also for satellite gravimetry observations from GRACE and GRACE-FO, the signal-to-noise ratio is low and the noise floor strongly dominates the time series in dry areas. To classify dry (desert) regions, we rely on the soil moisture signal variability, that is, the root mean square (RMS) of the daily time series in each grid cell. We set a low variability threshold of twice the mean RMS of a test region in the Sahara desert, which has minimal day-to-day soil moisture variations. To define the mask using this criterion, we used the SMOS L3 data product. Other SSM data products yielded similar results. Furthermore, snow cover and frozen soil prevent satellites from measuring soil moisture because the dielectric constant of snow and frozen water is very different from that of liquid water (Wagner, 1998). Regions with snow and frozen ground throughout large parts of the year were not spatially masked out, but we excluded the affected days from the analysis. To this end, soil temperature (T_S) and snow water equivalent (SWE) estimates of the Global Land Data Assimilation System NOAH (GLDAS NOAH) were used. Observations taken under the conditions of frozen soil ($T_S < 0°\text{C}$) and snow cover ($\text{SWE} > 0$ mm) according to the simulation results were excluded. A similar approach is used by ESA CCI (Gruber et al., 2019).

The GRACE TWS data used in this study has spatial limitations that are also relevant to our analysis. The primary limitation is the coarse spatial resolution, which results in the non-independence of TWS grid cell values from neighboring cells. This lack of independence can lead to leakage effects (Longuevergne et al., 2013), which are particularly relevant in coastal areas so that oceanic and terrestrial mass changes cannot be separated unambiguously. A more comprehensive discussion and a map highlighting continental areas affected by ocean leakage can be found in Eicker et al. (2020) (Figure S4 in Supporting Information S1). We used this map in our study to mask out areas that are largely affected by ocean leakage. GRACE-derived TWS also encompasses storage variations in other compartments than soil moisture and groundwater, for example, glaciers or surface water bodies, which are not directly of interest for the present study. For an identification of such regions including their effect on neighboring cells by leakage, we refer to Jensen et al. (2020) (Figure S2 in Supporting Information S1) but do not explicitly exclude such areas from our analyses.

19447973, 2025, 8, Downloaded from https://agupubs.onlinelibrary.wiley.com/doi/10.1029/2024WR039321 by Hafencity Universitaet Hamburg, Wiley Online Library on [18/02/2026]. See the Terms and Conditions (https://onlinelibrary.wiley.com/terms-and-conditions) on Wiley Online Library for rules of use; OA articles are governed by the applicable Creative Commons License

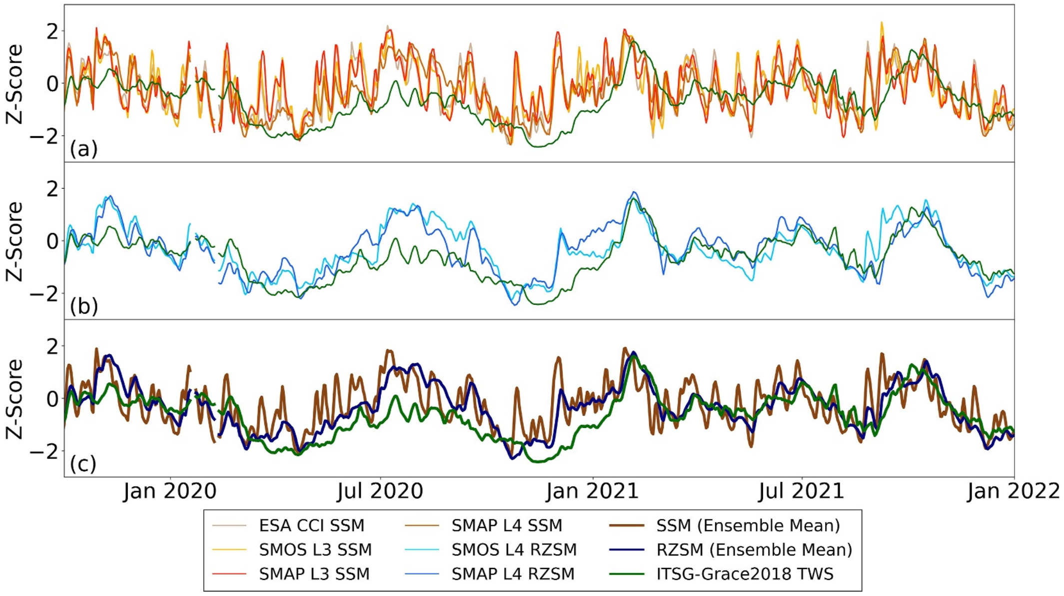

Figure 2. De-seasonalized time series for an example grid cell in the south of Brazil (29°S, 54°W). (a) Surface soil moisture (SSM) of ESA CCI, SMOS L3, SMAP L3, SMAP L4, and TWS from GRACE. (b) Root zone soil moisture (RZSM) of SMOS L4, SMAP L4, and TWS data from GRACE. (c) Ensemble mean of all SSM data sets (light brown) and RZSM data sets (dark blue) and TWS from GRACE. The individual time series are plotted as well, with a smaller line width.

4. Methods and Results

In the following, the methodology for investigating drought dynamics is described step by step and each calculation step is directly illustrated by results for one exemplary grid cell (Sections 4.1 to 4.3). Afterward, the methodology is extended to the global scale (Section 4.4).

4.1. Quantifying Water Storage Deficits

The standardized de-seasonalized signals for all products are illustrated in Figure 2 for an exemplary grid cell (29° S, 54° W) in the Brazilian state of Rio Grande do Sul, located in the south of Brazil within the Rio de la Plata river basin. This region experienced severe droughts from 2019 to 2022, as detailed in the European Commission report by Naumann et al. (2023). It is evident that the surface soil moisture data from SMOS L3, SMAP L3, ESA CCI and SMAP L4 exhibit fast dynamics with marked fluctuations of the soil water content and with quick recoveries from below-average moisture conditions (Figure 2a). In comparison, the storage fluctuations are smaller in the root zone time series from SMOS L4 and SMAP L4 (Figure 2b) and are further dampened in the entire water column time series of TWS from GRACE. Not only are fluctuations dampened when considering larger integration depths, but also the tendency toward more long-lasting water deficit conditions with a larger soil depth is evident, in particular for the recovery period between July 2020 and January 2021. With larger integration depths, also the onset and the gradual storage loss of storage deficit periods over time is dampened and delayed. While there are some differences between the individual data sets, the ensemble mean of all SSM data sets (light brown) and of all RZSM data sets (dark blue), along with TWS, clearly illustrates the distinct dynamics of water storage for the different integration depths (Figure 2c). Additional examples of time series for other grid cells worldwide are shown in Supporting Information S1. Figures S5 and S6 show results of the drought in New South Wales, Australia in 2019 (Bureau of Meteorology, 2019; Nguyen et al., 2021). Figures S7 and S8 in Supporting Information S1 show results of the drought in the Mekong river basin from 2019 to 2021 (Keovilignavong et al., 2023; Mekong River Commission, 2022). These are in line with the general results of depth dependencies of storage dynamics as presented here for the example of southern Brazil.

As mentioned before, to analyze the dynamics of droughts, we take a broad definition of water storage droughts in this study by considering all negative values of the standardized de-seasonalized water storage time series per grid cell, referred to herein as storage deficit. Furthermore, instead of focusing on a limited number of specific drought occurrences, we take a comprehensive approach that includes all occurrences of storage deficits, even in cases

19447973, 2025, 8, Downloaded from https://agupubs.onlinelibrary.wiley.com/doi/10.1029/2024WR039321 by Hafencity Universitaet Hamburg, Wiley Online Library on [18/02/2026]. See the Terms and Conditions (https://onlinelibrary.wiley.com/terms-and-conditions) on Wiley Online Library for rules of use; OA articles are governed by the applicable Creative Commons License

19447973, 2025, 8, Downloaded from https://agupubs.onlinelibrary.wiley.com/doi/10.1029/2024WR039321 by Hafencity Universitaet Hamburg, Wiley Online Library on [18/02/2026]. See the Terms and Conditions (https://onlinelibrary.wiley.com/terms-and-conditions) on Wiley Online Library for rules of use; OA articles are governed by the applicable Creative Commons License

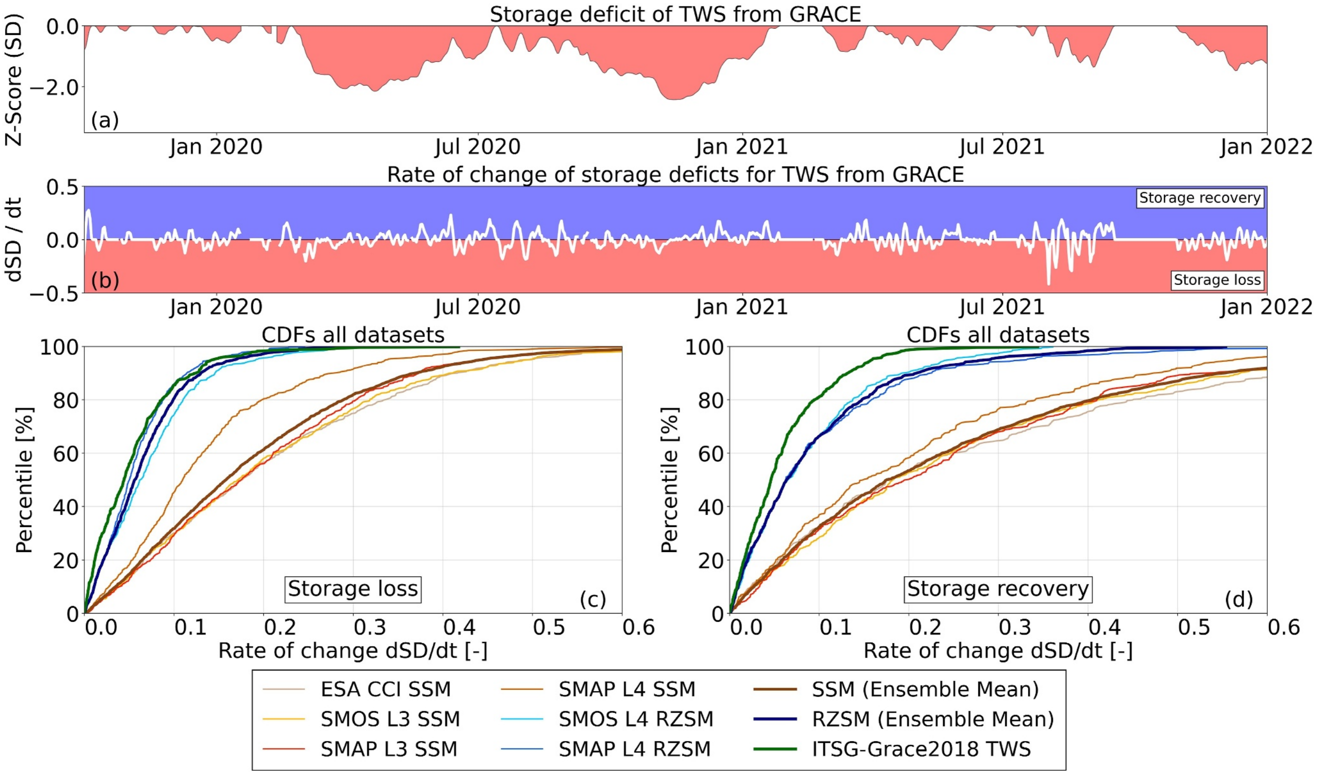

Figure 3. (a) Time series of TWS storage deficit for the exemplary grid cell in the south of Brazil (29°S, 54°W). (b) TWS rate of change time series (dSD/dt). (c) Cumulative distribution function (CDF) of storage loss rate of change values for all data sets. (d) CDF of storage recovery rate of change values for all data sets.

where the duration of a particular deficit in the time series is quite short. The metric used to quantify the storage deficits is based on a statistical method proposed by Thomas et al. (2014). The temporal evolution of storage deficits, encompassing storage loss and recovery over time, is determined by estimating the time derivative of the storage deficit dSD/dt. The computation is performed using the backward difference method:

$$\frac{dSD}{dt}(t) = SD_t - SD_{t-1} \tag{4}$$

To illustrate the method, we again show the results for the exemplary grid cell in Brazil. In Figure 3a, the storage deficit of TWS from GRACE/GRACE-FO during the drought period from 2019 onward is displayed, corresponding to the negative values of the green curve in Figure 2. The time derivative of the storage deficit describes the rate of change in the storage compartment over time (the rate of change here represents the change of the standardized unit-less values of the z-score SD per day). In the visual representation, values in the red area indicate storage loss (negative changes), while values in the blue area represent storage recovery (positive changes). A straight line around zero or gaps indicate that there was no storage deficit during that time.

For the further analyses, we assume that the entire rate of change (dSD/dt) time series of a grid cell represents the typical range of values during storage deficits. An empirical cumulative distribution function (CDF) of the rate of change time series is used to characterize the dynamics of droughts. The CDFs of all data sets are categorized into storage loss (Figure 3c) and storage recovery values (Figure 3d) because the number of loss and recovery time steps can be different and in order to distinguish between storage recovery and loss dynamics. It is important to note that storage loss values are typically negative. However, for visualization purposes, the absolute values are considered to make them more easily comparable to the positive values of storage recovery. The more to the right the values are, the faster the rate of change is during deficits. Upon closer examination of the CDFs of the storage recovery values (bottom right figure), it is evident that the recovery rates of SSM are the fastest, RZSM recovers more slowly from storage deficits, and the slowest rate of change are observed for TWS from GRACE. This indicates that the recovery time from droughts is much faster in the upper layers compared to the recovery of the

19447973, 2025, 8, Downloaded from https://agupubs.onlinelibrary.wiley.com/doi/10.1029/2024WR039321 by Hafencity Universitaet Hamburg, Wiley Online Library on [18/02/2026]. See the Terms and Conditions (https://onlinelibrary.wiley.com/terms-and-conditions) on Wiley Online Library for rules of use; OA articles are governed by the applicable Creative Commons License

entire water column from the surface to the subsurface. When looking at the rate of change values during storage loss periods (bottom left figure), we observe a similar pattern, but the difference is that both SMAP Level 4 products (SSM and RZSM) in this case are slower than the other surface soil moisture or root zone data. The SMAP Level 4 RZSM is even very close to the dynamics of storage loss from TWS. These different characteristics of the SMAP L4 water deficit change rates may be due to the particular properties of the hydrological model into which the observations are assimilated, such as model structure or model equations that govern the redistribution of water in the soil column, including losses by evapotranspiration or percolation. Also, the results may indicate that during the assimilation process, a rather small weight is given to the observations, as seen in particular by the large differences between SMAP L3 SSM observations and SMAP L4 SSM after assimilation.

Furthermore, Figure 3 shows that the dynamics of storage loss tend to be slower than the storage change rates during recovery periods. However, it should be noted that these results relate to one specific grid cell only and may vary in other locations, see Section 4.4.

4.2. CDF Ratios Between Data Sets

Going beyond the visual comparison of the CDFs (Figures 3c and 3d) for quantifying the CDF differences in a comprehensive global analysis, one approach is to select specific percentile values for comparison. To include the entire spectrum of CDF differences, we calculate the ratio of a range of percentiles (from the 1st to the 99th percentile) between TWS and the different soil moisture data sets. When dividing the percentile value of a soil moisture data set by the same percentile value of the TWS change rate, values greater than 1 indicate that the percentile of the soil moisture data set recovers faster than TWS, while a value below 1 indicates that TWS changes are faster. The larger the ratio, the faster the soil moisture data set recovers from storage deficits compared to TWS. It should be noted that this comparison of CDFs in terms of ratios is only possible when all data are standardized.

For the example of the 50th percentile of storage recovery, the ratios between surface soil moisture and TWS are 3.3–4.3 (SMOS L3 = 3.9, SMAP L3 = 4.3, SMAP L4 = 3.3, and ESA CCI = 4.0), while the ratios between RZSM and TWS are smaller with 1.3 (SMOS L4) to 1.4 (SMAP L4). For most data sets, the CDF ratios for storage loss are similar to those for storage recovery (SMOS L3 = 3.8, SMAP L3 = 3.9, ESA CCI = 3.9, SMOS L4 = 1.4), with the exception of both SMAP L4 data sets that result in considerably smaller ratios (SSM/TWS = 2.5, RZSM/TWS = 1.1).

For storage recovery, the mean value of all ratio values are very similar from the 10th and 90th percentiles ($\overline{x}_r$, step of 1%, in total 80 values) leads to ratios in a similar range than for the 50th percentile, with values between 3.3 and 4.2 for the surface soil moisture data sets (SMOS L3 ($\overline{x}_r = 4.1$), SMAP L3 ($\overline{x}_r = 4.0$), SMAP L4 ($\overline{x}_r = 3.3$, and ESA CCI $\overline{x}_r = 3.8$). The mean ratio for the root zone data is again significantly lower (SMOS L4: $\overline{x}_r = 1.4$; SMAP L4 $\overline{x}_r = 1.4$). The mean ratios for the storage loss CDF on the other hand, are slightly higher for ESA CCI ($\overline{x}_r = 4.5$), SMOS L3 ($\overline{x}_r = 4.4$), SMAP L3 ($\overline{x}_r = 4.5$), and SMOS L4 ($\overline{x}_r = 1.5$)), while they are lower for the two data assimilated SMAP L4 data sets (surface $\overline{x}_r = 3.0$, root zone $\overline{x}_r = 1.1$).

4.3. Recovery Time From Storage Deficit

As another approach to compare the different storage data sets, we estimate the median drought recovery time $(RT_{y,d})$ for any daily storage deficit $(SD_{y,d}i)$ by

$$RT_{y,d} = \frac{|SD_{y,d}|}{r_{50}}. \tag{5}$$

where r_{50} is the 50th percentile (median) of the storage change CDF of the respective data set. Using this approach allows for estimating a probabilistic recovery time for each day within a storage deficit period assuming a linear recovery from the day of the deficit. It is, of course, important to mention that real-world conditions may not follow such a linear pattern. However, the approach provides a first-order idea of the expected duration of a drought to be used for the comparison of the different storage data sets and of regional differences. Figure 4 illustrates the recovery times RT for the example grid cell in southern Brazil. While the maximum z-score of the storage deficit is quite similar for all data sets with values of about −2.0 (see Figure 2), the recovery time is scaled by the 50th percentile rate of change, which is different for each data set. Consequently, we observe that the

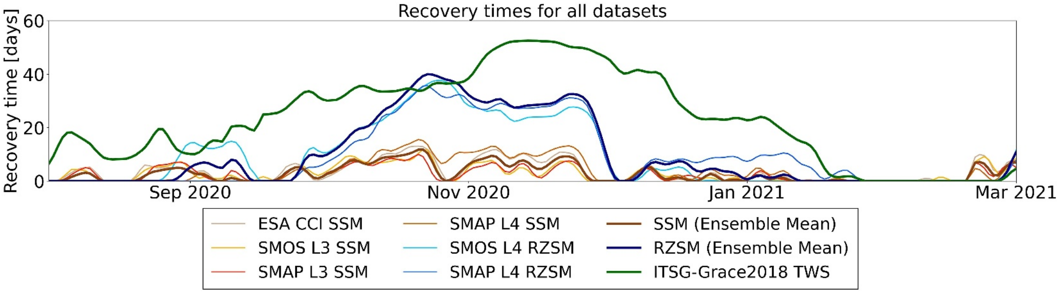

Figure 4. Time series of expected recovery times when considering the 50th percentile of storage recovery rates from the CDFs in Figure 3d for an exemplary grid cell in the south of Brazil: 29°S, 54°W.

recovery times for surface soil moisture data are much faster compared to the data sets of root zone soil moisture and even faster than the TWS data from GRACE. These patterns are corroborated by the mean $\bar{x}$ and maximum $x_{\max}$ of these recovery times for the entire time series in Table 1 (Figure 4 displays just a shorter snapshot). We can observe this effect again and see faster recovery times in the surface layer ($\bar{x} \sim 4$ d and $x_{\max} \sim 10$–15 d), which are prolonged in the deeper layers ($\bar{x} \sim 12$ d and $x_{\max} \sim 36$ d in the root zone, and $\bar{x} \sim 17$ d and $x_{\max} \sim 52$ d in the TWS). Additionally, recovery time ratios are calculated between the soil moisture data sets and TWS. The ratios are similar to those calculated from the CDFs (Section 4.2) for the SMAP L4 and SMOS L4 data, while for the SMOS L3, SMAP L3, and ESA CCI data set, the ratios are slightly higher. An added advantage of utilizing recovery times as a metric is that there is no need to standardize the data in advance. Comparisons and calculations can be conducted solely based on the anomaly signal.

4.4. Global Analysis

So far, the analysis approach was illustrated on the basis of only one exemplary grid cell and shall now be extended to the global scale. The global maps in Figure 5 show the average recovery times from storage deficit following Equation 5 on the 1° continental grid. The analysis excluded regions affected by desert conditions (where noise dominates the signal) and ocean leakage (where ocean signal corrupt TWS data from GRACE/GRACE-FO). For the remaining grid cells, the global cumulative distribution functions (CDF) of the cell-based recovery time values are depicted in Figure 7a. Both the maps and the CDFs make it evident that also on the global scale the mean recovery time is substantially shorter for the four SSM products than for RZSM and TWS, typically in the range of 5 and 10 days with a global median value of the ensemble mean map of 6.4 days. The data assimilated SMAP L4 SSM data shows slightly higher recovery times, with some regions exceeding 10 days. In contrast, RZSM exhibits longer recovery times related to deeper and longer travel times of infiltrating water and the larger storage volume to be filled compared to SSM, with a median value of the ensemble mean map of 14.0 days. Noticeable differences are observed between the SMOS and SMAP root zone data sets, particularly in rain forests and northern latitude regions. The longer recovery times for the SMAP L4 root zone product are particularly evident. TWS generally has the longest recovery times. The global median value of all grid cells is

Table 1
Average and Maximum Recovery Times for the Different Surface Soil Moisture (SSM), Root-Zone Soil Moisture (RZSM) Products, and for TWS

Data set	$\bar{x}$ [days]	$x_{\max}$ [days]	Ratio $\bar{x}$ [−]	Ratio $x_{\max}$ [−]
ESA CCI SSM	3.8	13.1	4.5	4.0
SMOS L3 SSM	3.5	11.8	4.9	4.5
SMAP L3 SSM	3.3	10.8	5.2	4.9
SMAP L4 SSM	4.8	15.5	3.5	3.4
SMOS L4 RZSM	12.5	37.7	1.3	1.4
SMAP L4 RZSM	12.0	35.7	1.4	1.5
ITSG-Grace2018 TWS	17.1	52.6	–	–

Note. Additionally, the ratios of the soil moisture recovery times w.r.t to TWS are shown.

19447973, 2025, 8, Downloaded from https://agupubs.onlinelibrary.wiley.com/doi/10.1029/2024WR039321 by Hafencity Universitaet Hamburg, Wiley Online Library on [18/02/2026]. See the Terms and Conditions (https://onlinelibrary.wiley.com/terms-and-conditions) on Wiley Online Library for rules of use; OA articles are governed by the applicable Creative Commons License

19447973, 2025, 8, Downloaded from https://agupubs.onlinelibrary.wiley.com/doi/10.1029/2024WR039321 by Hafencity Universitaet Hamburg, Wiley Online Library on [18/02/2026]. See the Terms and Conditions (https://onlinelibrary.wiley.com/terms-and-conditions) on Wiley Online Library for rules of use; OA articles are governed by the applicable Creative Commons License

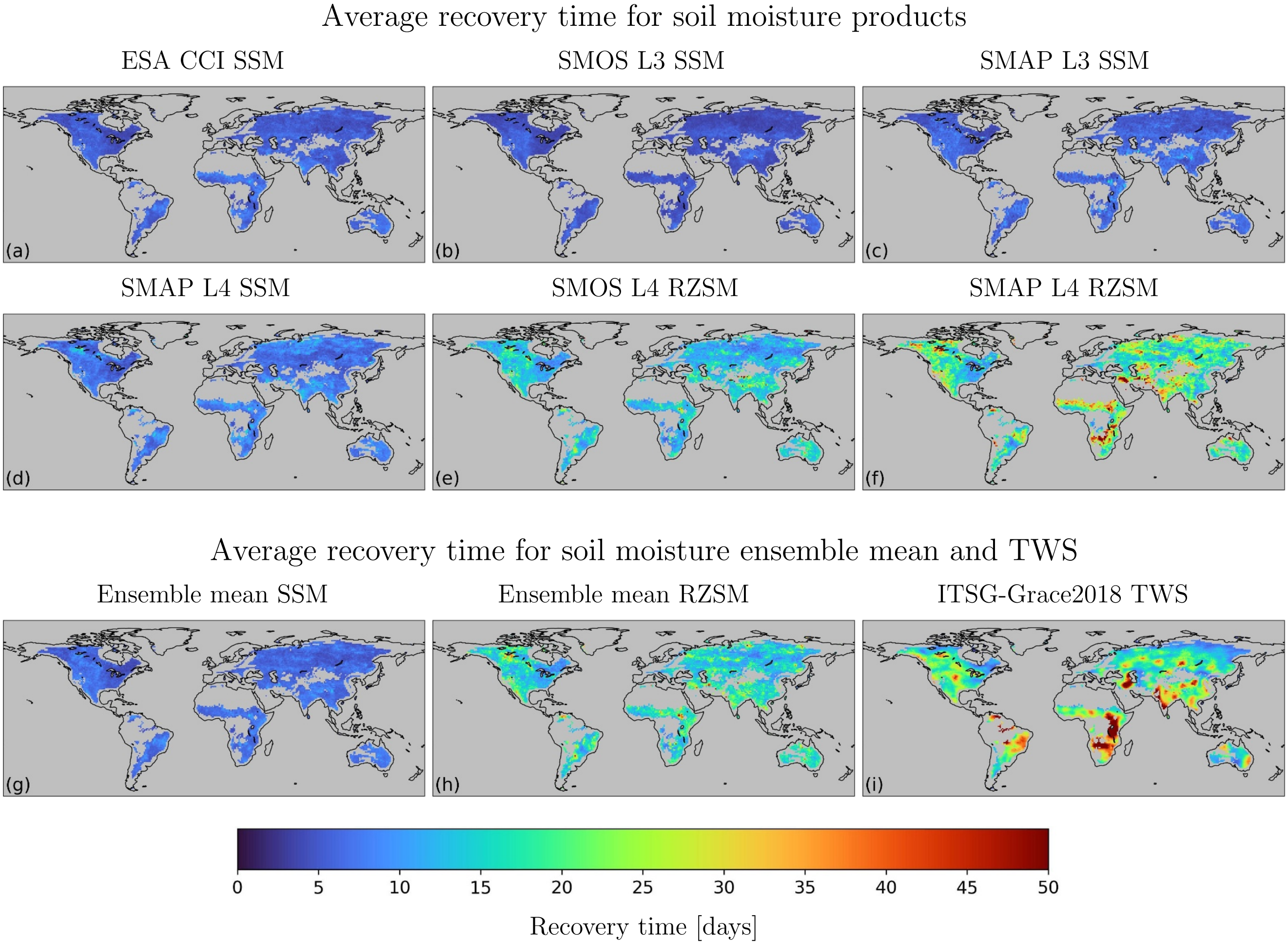

Figure 5. Average recovery times for storage deficits (04.2015–12.2022) computed for each grid cell assuming the 50th percentile of the daily rate of storage increase during deficit periods. Maps (a–d) surface soil moisture products; maps (e) and (f) root zone soil moisture products; maps (g) and (h) ensemble mean of SSM and RZSM; (i) TWS.

21.0 days. Regions with the longest recovery times include southern and eastern Africa, India, and the Tigris-Euphrates river system southwest of the Caspian Sea, but other regions, such as the eastern regions of Brazil and Australia, show significant differences in recovery times between TWS and RZSM. There are some regions, where the recovery times of SMAP L4 RZSM are even longer than those of TWS, particularly in parts of the northern latitude regions of Canada and Russia and in arid regions south of the Sahara.

We would like to recall the fact that data gaps in the SSM time series were filled by linear interpolation (see Section 3.1). To evaluate the effect of linear interpolation, we performed a simulation based on SMAP L4 SSM product as a reference, which shows similar short-periodic variability as the other SSM products, but does not contain data gaps. We then artificially introduced the same gaps present in the other SSM products (SMOS L3, SMAP L3, ESA CCI) into the SMAP L4 SSM data set and applied our gap-filling procedure and subsequent estimation of the recovery times. For ESA CCI with only a few data gaps, there is hardly any difference in the results. For SMOS and SMAP L3 data gaps our findings indicate that linear interpolation does introduce minor differences. The smoothing effect of linear interpolation results in a slightly slower recovery process, as expected, due to reduction of inherent variability. While for individual grid cells this can amount to about 2–3 days of recovery time, the average delay is around one day. This implies that the CDFs of the recovery times for these SSM data sets in Figure 7 would be slightly further to the left in case of no data gaps, resulting in a slightly stronger difference between recovery times of SSM and RZSM. However, the overall patterns and qualitative conclusions remain unaffected by the linear interpolation.

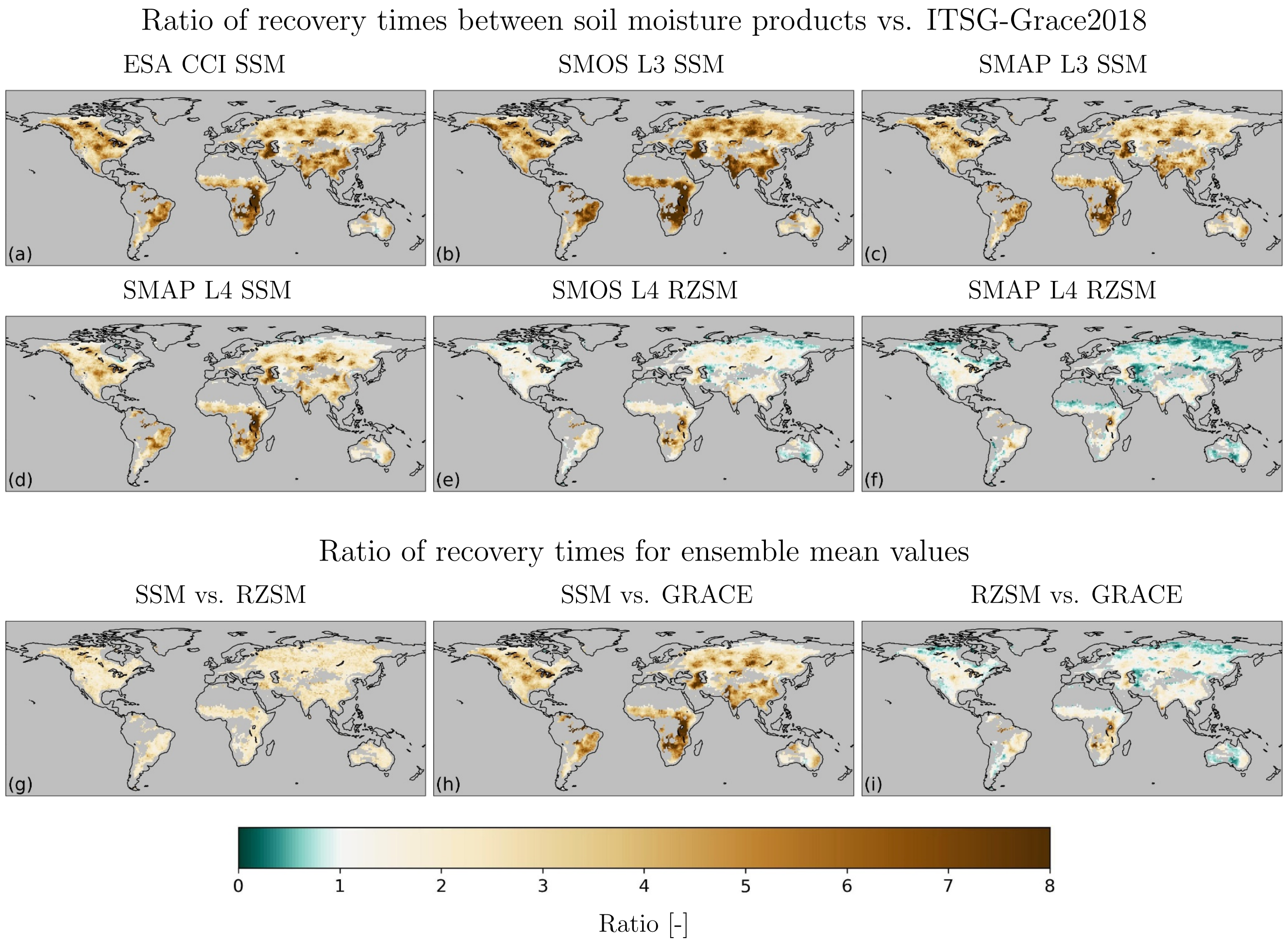

Figure 6. Global maps of the ratios of recovery times between TWS and the respective soil moisture products. Maps (a–d): surface soil moisture products; maps (e) and (f): root zone soil moisture products; maps (g–i) ensemble mean ratios: (g) SSM and RZSM, (h) SSM and TWS, and (i) RZSM and TWS. Values above 1 (depicted in brownish color) indicate faster storage recovery for the soil moisture product, while values below 1 (shown in greenish color) suggest faster storage recovery for TWS.

As mentioned in Section 3.1, another potential limitation of the performed analysis is the different native spatial resolution of the soil moisture and TWS data sets. To address this, we additionally computed recovery times after converting the soil moisture data sets into a spherical harmonics representation up to degree $n = 40$ (approximately 500 km) matching the spatial resolution of the GRACE data. The results are shown in Figures S9 and S10 in Supporting Information S1. For surface soil moisture products, the recovery times computed from this harmonized resolution showed negligible differences to the original $1^\circ \times 1^\circ$ grid. For root-zone soil moisture, particularly for SMAP L4 RZSM, shorter recovery times were observed after harmonization (see Figure S9 in Supporting Information S1). This can also be seen when comparing the CDFs of the recovery times (Figure S10 in Supporting Information S1), in which the CDF of the spherical harmonic result for SMAP L4 RZSM is further to the left and thus further apart from the TWS line compared to the corresponding result shown in Figure 7. This means that when aligning the spatial resolution between TWS and soil moisture data, the differences between TWS and RZSM recovery times become even more pronounced. However, the qualitative conclusion of our study, that is the relative order of the CDFs, is not influenced by the choice of the spatial resolution suggesting that the spatial smoothing inherent in GRACE data does not bias our findings. Therefore, we retain the $1^\circ \times 1^\circ$ resolution for soil moisture data as a practical compromise between their finer native resolutions and the coarser effective resolution of GRACE-based TWS, while avoiding additional unnecessary smoothing of the soil moisture signals.

Along the lines of the numbers provided in Table 1, we again established TWS as the reference and computed the ratios of average recovery times for each soil moisture product relative to TWS for each investigated grid cell (Figures 6a–6f). In addition to the ratios of the individual soil moisture products, also the ratios of the two

19447973, 2025, 8, Downloaded from https://agupubs.onlinelibrary.wiley.com/doi/10.1029/2024WR039321 by Hafencity Universitaet Hamburg, Wiley Online Library on [18/02/2026]. See the Terms and Conditions (https://onlinelibrary.wiley.com/terms-and-conditions) on Wiley Online Library for rules of use; OA articles are governed by the applicable Creative Commons License

19447973, 2025, 8, Downloaded from https://agupubs.onlinelibrary.wiley.com/doi/10.1029/2024WR039321 by Hafencity Universitaet Hamburg, Wiley Online Library on [18/02/2026]. See the Terms and Conditions (https://onlinelibrary.wiley.com/terms-and-conditions) on Wiley Online Library for rules of use; OA articles are governed by the applicable Creative Commons License

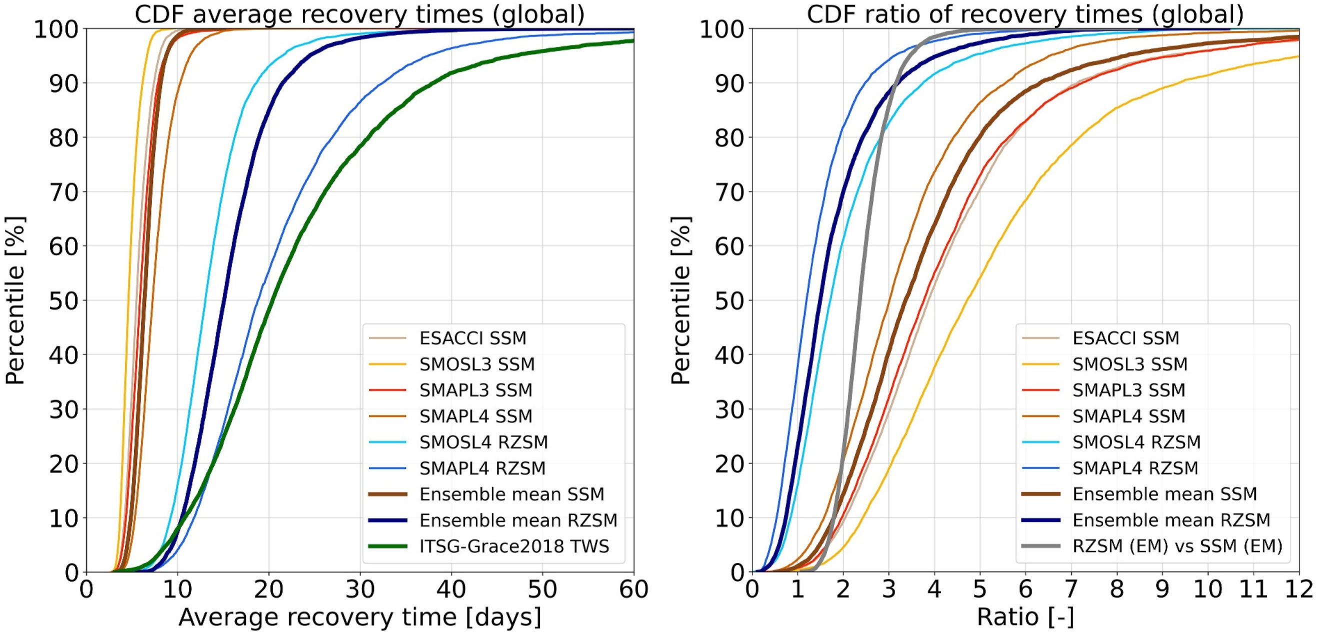

Figure 7. (a) Cumulative distribution functions (CDF) of cell-based mean recovery time values. Recovery times are calculated by the 50th percentile of the rate of change values, describing the storage recovery during water deficit periods. (b) Cumulative distribution functions (CDF) of cell-based ratios between TWS from GRACE and the respective soil moisture product. Both CDFs are restricted to grid cells defined as "area suited for analysis" in Figure 1.

ensemble means of SSM and RZSM with respect to TWS are plotted (h and i) and the ratio of the SSM ensemble mean with respect to the ensemble mean of the RZSM products (g). Corresponding CDFs of the cell-based ratio values are presented in Figure 7b with the fat brown and green lines representing the ensemble means of SSM and RZSM. Ratio values exceeding 1 indicate faster storage recovery for the respective soil moisture product, whereas values below 1 suggest faster storage recovery for TWS. In general, all surface soil moisture products exhibit ratios substantially above 1, with the majority (CDF range between percentiles from 20% to 80%) falling between a ratio of 2 and 6. This is also confirmed by the results of the respective ensemble mean (Figure 6h, median grid value equal to 3.1). Notably, the ratios between SMOS L3 SSM and TWS are higher compared to the other SSM products, which could partly be attributed to a higher noise level in the data set resulting in faster fluctuations of the time series and thus spuriously shorter recovery times. The ratios of SMAP L3 SSM and ESA CCI are about the same, but the SMAP L4 SSM product has smaller ratios. The RZSM ratios are notably smaller than SSM ratios, with the majority falling in the range of 1–3, with a median value of 1.5. Additionally, a higher fraction of values below 1 is observed for RZSM, indicating slower recovery than TWS. While for SMOS L4 RZSM this applies to approximately 15% of all grid cells, for SMAP L4 RZSM, 35%–40% of all grid cells exhibit ratios smaller than 1. As indicated above, these values are primarily located in the northern latitudes or in arid regions such as the Sahel region, large parts of Australia, the southwestern United States, and Central Asia. Overall, in other regions, the SMOS L4 RZSM ratios are slightly higher than SMAP L4 RZSM ratios, suggesting that differences in the methods used to generate the root zone data may play a role in the variability of the storage recovery. The ratio of the SSM versus the RZSM recovery times (Figure 6g, median grid value of 2.4) confirms the slower dynamics of RZSM. While these ratios offer a convenient and intuitive way to express the relative differences in recovery dynamics between variables and to illustrate spatial patterns of hydrological dynamics, they should be interpreted with caution. Each ratio represents the division of two quantities that are both subject to considerable uncertainties due to data resolution and processing techniques. Consequently, these uncertainties are propagated and accumulated in the ratios at the grid cell level.

5. Discussion and Conclusions

The results shown here demonstrate that satellite products with daily resolution, particularly satellite gravimetry from GRACE/GRACE-FO and satellite soil moisture data, can quantify the dynamics of drought cascades across the entire depth of the water column to comprehensively analyze sub-surface drought propagation processes.

Understanding these dynamics is crucial for effective water resource management and mitigating the impacts of droughts. Overall, the concept of drought propagation and recovery across different soil depths can well be recognized in the results.

Through a detailed examination of storage deficits and recovery times across various integration depths in the subsurface, from surface soil moisture to the entire water column represented by TWS, this study reveals differences in drought dynamics. The findings indicate that surface soil moisture exhibits faster evolution and recovery times compared to deeper soil layers and TWS, suggesting that near-surface soil moisture data could provide valuable insights for the early detection and monitoring of droughts. Moreover, the comparison of recovery times and ratios between different soil moisture products and TWS highlights the importance of considering different integration depths below the surface in drought monitoring and prediction. While TWS data from GRACE provide valuable information on the longer lasting features of hydrological droughts, surface soil moisture and root-zone soil moisture data offer more rapid and localized insights on meteorological and agricultural droughts, particularly during the early stages of drought events.

The results presented here show recovery times that are on average around 1.6 times longer (median value of recovery time ratios shown in Figure 6i) for TWS compared to RZSM. Similar relations of drought dynamics can be found, for example, in Farahmand et al. (2021), who conclude an average drought duration of 18.5 months for modeled SM including SSM and RZSM versus 27.5 months for TWS for four major US drought case studies, albeit with large variations among the different drought events. Time series shown in Rossi et al. (2023) allow an estimation of the duration of individual drought events of, for example 14 months (sub-surface SM) versus 21 months (TWS) for a drought event in Cerrado, Brazil. This is also well within the range of our findings on the recovery times from water storage deficits. In Entekhabi (2023), the delay and dampening effects of soil moisture and terrestrial water storage are analyzed for the continental United States, see Figure 5 of their manuscript. These dampening effects may be related to our rate of change values, as both reflect the reduced variability in deeper soil layers. However, a direct one-to-one comparison remains challenging due to the differing physical interpretations and sensitivities of the respective variables. The results from Entekhabi (2023) indicate that SMAP soil moisture data is dampened by approximately 25%–30%, while GRACE TWS experiences a stronger dampening effect of up to 80% relative to meteorological drought signals derived from precipitation. This corresponds to a ratio between SMAP and GRACE of approximately 0.31–0.37. Similarly, in our analysis, the average recovery time for the United States is around 6 days for SMAP L3 SSM and 20 days for GRACE TWS, resulting in a ratio of approximately 0.30. Despite the differences in methodologies, this could suggest that our findings align well with the observed dampening effect reported in Entekhabi (2023).

In our results, SMAP L4 RZSM exhibits slower rates of change and longer recovery times than TWS in some regions. This is a conceptually unexpected result at the first glance. For areas where soil moisture and groundwater are the dominant storage compartments, such as south of the Sahara, this might be attributed to the too slowly reacting soil water dynamics in the SMAP assimilation model. Other affected regions are in the northern latitudes. Here the temporal masking of the soil moisture products during frozen soil conditions leads to inconsistencies with the time coverage of the TWS time series, which may influence the results. In the overlapping time spans in the summer months, time series of SMAP L4 RZSM show a substantially smoother behavior and less temporal variability compared to TWS, which is in contrast to the findings in other regions. For these high latitude regions, Reichle et al. (2023, Figure 29c) show very small RZSM observation increments in the SMAP L4 data assimilation scheme as indicated by the temporal standard deviation of these increments. This means that in these regions, the satellite observations provide only minimal corrections to the model forecast of RZSM. Thus, the too slow RZSM dynamics compared to TWS are driven almost entirely by the underlying hydrological model. The discussion above and the results of our study in general suggest the potential of the remote sensing data sets with different integration depths to help in evaluating or even improving the infiltration and percolation schemes of hydrological models. Also, the data might be of use for tuning empirical model parameters such as those of exponential filters or other transfer functions that are used for the depth-extrapolation of SSM to RZSM (e.g., Rasche et al., 2024).

The results show that recovery time increases with deeper sub-surface integration depths. While the global spatial distribution of recovery times (Figure 5) for the soil moisture products is rather homogeneous, there are marked spatial variations of recovery times when considering TWS. For the soil moisture products, a uniform depth is assumed globally (5 cm for SSM and 1 m for RZSM), leading to a comparatively homogeneous behavior

19447973, 2025, 8, Downloaded from https://agupubs.onlinelibrary.wiley.com/doi/10.1029/2024WR039321 by Hafencity Universitaet Hamburg, Wiley Online Library on [18/02/2026]. See the Terms and Conditions (https://onlinelibrary.wiley.com/terms-and-conditions) on Wiley Online Library for rules of use; OA articles are governed by the applicable Creative Commons License

19447973, 2025, 8, Downloaded from https://agupubs.onlinelibrary.wiley.com/doi/10.1029/2024WR039321 by Hafencity Universitaet Hamburg, Wiley Online Library on [18/02/2026]. See the Terms and Conditions (https://onlinelibrary.wiley.com/terms-and-conditions) on Wiley Online Library for rules of use; OA articles are governed by the applicable Creative Commons License

everywhere which is dominated by vertical water transport processes. For TWS, in contrast, the hydrologically active zone, in which relevant magnitudes of water storage change can occur, may differ considerably between regions depending, for example, on the depth to bedrock or the thickness of unconsolidated sediments. Another aspect are heterogeneous groundwater dynamics governed by the regional hydrogeology and associated lateral groundwater transport. These factors cause the recovery times to vary spatially much more markedly. To further explore the spatial variability of recovery times and their potential drivers, we performed a first-order qualitative analysis by comparing the CDFs of recovery times for zones of different environmental characteristics based on global data sets of topography (NOAA National Centers for Environmental Information, 2022), vegetation-based land cover (Friedl & Sulla-Menashe, 2022), Köppen-Geiger climate zones (Kottek et al., 2006), and soil clay fraction data from GLDAS (Rodell et al. (2004) as derived from global soil data sets from Reynolds et al. (2000)). The corresponding figures are shown in Figures S11–S14 in Supporting Information S1. However, identifying causality for the spatial patterns of recovery times from this comparison is inherently difficult due to the spatial co-occurrence of many environmental factors that may affect the actual hydrological processes in a complex way. Some tendencies that emerged from this analysis are the following: Recovery times tend to be shorter in lowland regions than in higher elevation zones particularly for TWS and root-zone soil moisture, possibly due to the convergence of lateral water flow in the lowlands. As an example of differences between vegetation types, grasslands generally exhibited longer recovery times than savannas, suggesting a role of larger rooting depth and soil structure with higher macro-porosity in savannas due to a higher tree coverage. The latter, in turn, may favor the faster water transport into larger depths and thus a quicker storage recovery after dry periods in savanna regions. Climate zones showed distinct signatures, with equatorial regions displaying slower recovery, while warm temperate zones recovered more quickly. Furthermore, with respect to soil properties, here soil texture, higher clay fractions are associated with slower recovery times at the global scale, possibly due to lower infiltration capacities and retarded vertical water transport in soils with higher clay content. It should be stressed again that these are preliminary results of a first-order univariate analysis and a much more elaborated multi-factorial study is needed in future work to disentangle the complex interplay of various environmental factors on the subsurface storage dynamics and recovery rates.

Further research should also focus on improving the integration of satellite gravimetry and soil moisture data to enhance the accuracy and reliability of drought monitoring systems. Joint assimilation of surface soil moisture and TWS into hydrological models has already proven very valuable (Tangdamrongsub et al., 2020) and holds further potential in improving the simulation of water storage in the subsurface due to the distinct sensitivity of the two data types to water storage dynamics in different soil depths.

Furthermore, continued advancements in satellite remote sensing and data analysis techniques offer great potential for enhancing our understanding of drought dynamics and improving drought management strategies. Ongoing improvements to the GRACE/-FO data processing and next-generation gravity missions such as the MAGIC constellation of two GRACE-like missions operating simultaneously at differently inclined orbits (Daras et al., 2023), give prospect to an increase of the temporal and spatial resolution of satellite-based TWS data in the future. Also, the growing record of satellite soil moisture products provides a constantly increasing length of overlapping time series. This, in turn, will allow for extending the analyses to longer drought durations and a larger number of events, ultimately leading to more robust results.

The global scope of study at hand exploits the advantage that satellite data are mostly available with global coverage. In future studies, the potential of the data sets can be enhanced with regional analyses that may also include in situ observations with different soil depths or with different integration depths such as networks of terrestrial gravimetry, Cosmic Ray Neutron sensors or other in situ soil moisture measurements.

Data Availability Statement

The daily GRACE and GRACE-FO data products of ITSG-Grace2018 are publicly available from TU Graz (Mayer-Gürr et al., 2018):

https://ftp.tugraz.at/outgoing/ITSG/GRACE/ITSG-Grace2018/daily_kalman/daily_n40/

https://ftp.tugraz.at/outgoing/ITSG/GRACE/ITSG-Grace_operational/daily_kalman/daily_n40/

19447973, 2025, 8, Downloaded from https://agupubs.onlinelibrary.wiley.com/doi/10.1029/2024WR039321 by Hafencity Universitaet Hamburg, Wiley Online Library on [18/02/2026]. See the Terms and Conditions (https://onlinelibrary.wiley.com/terms-and-conditions) on Wiley Online Library for rules of use; OA articles are governed by the applicable Creative Commons License

The ESA CCI soil moisture product can be downloaded from the ESA's Climate Change Initiative (CCI) web page (Dorigo et al., 2023):

http://catalogue.ceda.ac.uk/uuid/ff890589c21f4033803aa550f52c980c

Soil moisture products (Level 3 and Level 4) from the ESA's SMOS mission are made available by the Centre Aval de Traitement des Données SMOS (CATDS, 2022a, 2022b):

https://doi.org/10.12770/9cef422f-ed3f-4090-9556-b2e895ba2ca8

https://doi.org/10.12770/316e77af-cb72-4312-96a3-3011cc5068d4

Soil moisture products (Level 3 and Level 4) from NASA's SMAP mission are provided by the National Snow and Ice Data Center (NSIDC; O'Neill et al., 2023; Reichle et al., 2022):

https://doi.org/10.5067/4XXOGX0OOW1S and https://doi.org/10.5067/EVKPQZ4AFC4D.

Acknowledgments

A portion of this work was conducted at the Jet Propulsion Laboratory, California Institute of Technology, under contract with NASA. The authors would like to thank the editors for handling the manuscript and three anonymous reviewer for their constructive feedback. Open Access funding enabled and organized by Projekt DEAL.

References

AghaKouchak, A., Farahmand, A., Melton, F. S., Teixeira, J., Anderson, M. C., Wardlow, B. D., & Hain, C. R. (2015). Remote sensing of drought: Progress, challenges and opportunities. *Reviews of Geophysics*, *53*(2), 452–480. https://doi.org/10.1002/2014RG000456

Al Bitar, A., & Mahmoodi, A. (2020). *Algorithm theoretical basis document (ATBD) for the SMOS level 4 root zone soil moisture*. (Tech. Rep.). Zenodo. https://doi.org/10.5281/ZENODO.4298572

Bae, H., Ji, H., Lim, Y.-J., Ryu, Y., Kim, M.-H., & Kim, B.-J. (2019). Characteristics of drought propagation in South Korea: Relationship between meteorological, agricultural, and hydrological droughts. *Natural Hazards*, *99*(1), 1–16. https://doi.org/10.1007/s11069-019-03676-3

Barker, L. J., Hannaford, J., Chiverton, A., & Svensson, C. (2016). From meteorological to hydrological drought using standardised indicators. *Hydrology and Earth System Sciences*, *20*(6), 2483–2505. https://doi.org/10.5194/hess-20-2483-2016

Barros, A. P., Hodes, J. L., & Arulraj, M. (2017). Decadal climate variability and the spatial organization of deep hydrological drought. *Environmental Research Letters*, *12*(10), 104005. https://doi.org/10.1088/1748-9326/aa81de

Bergmann, I., & Dobslaw, H. (2012). Short-term transport variability of the Antarctic Circumpolar Current from satellite gravity observations. *Journal of Geophysical Research*, *117*(C5), C05044. https://doi.org/10.1029/2012JC007872

Bhardwaj, K., Shah, D., Aadhar, S., & Mishra, V. (2020). Propagation of meteorological to hydrological droughts in India. *Journal of Geophysical Research: Atmospheres*, *125*(22), e2020JD033455. https://doi.org/10.1029/2020JD033455

Blank, D., Eicker, A., Jensen, L., & Güntner, A. (2023). A global analysis of water storage variations from remotely sensed soil moisture and daily satellite gravimetry. *Hydrology and Earth System Sciences*, *27*(13), 2413–2435. https://doi.org/10.5194/hess-27-2413-2023

Bonin, J. A., & Chambers, D. P. (2011). Evaluation of high-frequency oceanographic signal in GRACE data: Implications for de-aliasing. *Geophysical Research Letters*, *38*(17), L17608. https://doi.org/10.1029/2011GL048881

Bureau of Meteorology. (2019). Special climate statement 72 - Dangerous bushfire weather in spring 2019. Retrieved from http://www.bom.gov.au/climate/current/statements/scs72.pdf

CATDS. (2022a). *CATDS-PDC L3SM filtered - 1 day global map of soil moisture values from SMOS satellite*. CATDS (CNES, IFREMER, CESBIO). https://doi.org/10.12770/9CEF422F-ED3F-4090-9556-B2E895BA2CA8

CATDS. (2022b). *CATDS-PDC L4SM RZSM - 1 day global map of root zone soil moisture values from SMOS satellite*. CATDS (CNES, IFREMER, CESBIO). https://doi.org/10.12770/316E77AF-CB72-4312-96A3-3011CC5068D4

Changnon, S. A. (1987). *Detecting drought conditions in Illinois*. Illinois State Water Survey. Circular No. 169.

Cheng, M., & Ries, J. (2017). The unexpected signal in GRACE estimates of C_{20. *Journal of Geodesy*, *91*(8), 897–914. https://doi.org/10.1007/s00190-016-0995-5

Crocetti, L., Forkel, M., Fischer, M., Jurečka, F., Grlj, A., Salentinig, A., et al. (2020). Earth observation for agricultural drought monitoring in the Pannonian Basin (southeastern Europe): Current state and future directions. *Regional Environmental Change*, *20*(4), 123. https://doi.org/10.1007/s10113-020-01710-w

Daras, I., March, G., Pail, R., Hughes, C., Braitenberg, C., Güntner, A., et al. (2023). *Mass-change and geosciences international constellation (MAGIC) expected impact on science and applications. Geophysical Journal International, ggad472*. Oxford University Press. https://doi.org/10.1093/gji/ggad472

Dobslaw, H., Bergmann-Wolf, I., Dill, R., Poropat, L., Thomas, M., Dahle, C., et al. (2017). A new high-resolution model of non-tidal atmosphere and ocean mass variability for de-aliasing of satellite gravity observations: AOD1B RL06. *Geophysical Journal International*, *211*(1), 263–269. https://doi.org/10.1093/gji/ggx302

Dorigo, W., Preimesberger, W., Hahn, S., van der Schalie, R., de Jeu, R., Kidd, R., et al. (2023). *ESA soil moisture climate change initiative (Soil_moisture_cci): Version 08.1 data collection*. NERC EDS Centre for Environmental Data Analysis. Retrieved from http://catalogue.ceda.ac.uk/uuid/ff890589c21f4033803aa550f52c980c

Dorigo, W., Scipal, K., Parinussa, R. M., Liu, Y. Y., Wagner, W., de Jeu, R. A. M., & Naeimi, V. (2010). Error characterisation of global active and passive microwave soil moisture datasets. *Hydrology and Earth System Sciences*, *14*(12), 2605–2616. https://doi.org/10.5194/hess-14-2605-2010

Dorigo, W., Wagner, W., Albergel, C., Albrecht, F., Balsamo, G., Brocca, L., et al. (2017). ESA CCI soil moisture for improved Earth system understanding: State-of-the art and future directions. *Remote Sensing of Environment*, *203*, 185–215. https://doi.org/10.1016/j.rse.2017.07.001

Eicker, A., Jensen, L., Wöhnke, V., Dobslaw, H., Kvas, A., Mayer-Gürr, T., & Dill, R. (2020). Daily GRACE satellite data evaluate short-term hydro-meteorological fluxes from global atmospheric reanalyses. *Scientific Reports*, *10*(1), 4504. https://doi.org/10.1038/s41598-020-61166-0

Entekhabi, D. (2023). Propagation in the drought cascade: Observational analysis over the continental US. *Water Resources Research*, *59*(9), e2022WR032608. https://doi.org/10.1029/2022WR032608

Entekhabi, D., Njoku, E. G., O'Neill, P. E., Kellogg, K. H., Crow, W. T., Edelstein, W. N., et al. (2010). The soil moisture active passive (SMAP) mission. *Proceedings of the IEEE*, *98*(5), 704–716. https://doi.org/10.1109/JPROC.2010.2043918

19447973, 2025, 8, Downloaded from https://agupubs.onlinelibrary.wiley.com/doi/10.1029/2024WR039321 by Hafencity Universitaet Hamburg, Wiley Online Library on [18/02/2026]. See the Terms and Conditions (https://onlinelibrary.wiley.com/terms-and-conditions) on Wiley Online Library for rules of use; OA articles are governed by the applicable Creative Commons License

Entekhabi, D., Yueh, S., O'Neill, P. E., Kellogg, K. H., Allen, A., Bindlish, R., et al. (2014). *SMAP handbook–soil moisture active passive: Mapping soil moisture and freeze/thaw from space*. JPL Publication. Retrieved from https://asf.alaska.edu/wp-content/uploads/2019/03/smap_handbook.pdf

Fan, Y. (2015). Groundwater in the Earth's critical zone: Relevance to large-scale patterns and processes. *Water Resources Research*, *51*(5), 3052–3069. https://doi.org/10.1002/2015WR017037

Farahmand, A., Reager, J. T., & Madani, N. (2021). Drought cascade in the terrestrial water cycle: Evidence from remote sensing. *Geophysical Research Letters*, *48*(14), e2021GL093482. https://doi.org/10.1029/2021GL093482

Friedl, M., & Sulla-Menashe, D. (2022). *MODIS/Terra+Aqua land cover type yearly L3 global 0.05Deg CMG V061*. NASA EOSDIS Land Processes Distributed Active Archive Center. https://doi.org/10.5067/MODIS/MCD12C1.061

Gouweleeuw, B. T., Kvas, A., Gruber, C., Gain, A. K., Mayer-Gürr, T., Flechtner, F., & Güntner, A. (2018). Daily GRACE gravity field solutions track major flood events in the Ganges–Brahmaputra Delta. *Hydrology and Earth System Sciences*, *22*(5), 2867–2880. https://doi.org/10.5194/hess-22-2867-2018

Gruber, A., Scanlon, T., van der Schalie, R., Wagner, W., & Dorigo, W. (2019). Evolution of the ESA CCI soil moisture climate data records and their underlying merging methodology. *Earth System Science Data*, *11*(2), 717–739. https://doi.org/10.5194/ESSD-11-717-2019

Huang, S., Li, P., Huang, Q., Leng, G., Hou, B., & Ma, L. (2017). The propagation from meteorological to hydrological drought and its potential influence factors. *Journal of Hydrology*, *547*, 184–195. https://doi.org/10.1016/j.jhydrol.2017.01.041

Jensen, L., Eicker, A., Stacke, T., & Dobslaw, H. (2020). Predictive skill assessment for land water storage in CMIP5 decadal hindcasts by a global reconstruction of GRACE satellite data. *Journal of Climate*, *33*(21), 9497–9509. https://doi.org/10.1175/JCLI-D-20-0042.1

Keovilignavong, O., Nguyen, T. H., & Hirsch, P. (2023). Reviewing the causes of Mekong drought before and during 2019–20. *International Journal of Water Resources Development*, *39*(1), 155–175. https://doi.org/10.1080/07900627.2021.1967112

Kerr, Y. H., Waldteufel, P., Wigneron, J.-P., Delwart, S., Cabot, F., Boutin, J., et al. (2010). The SMOS mission: New tool for monitoring key elements of the global water cycle. *Proceedings of the IEEE*, *98*(5), 666–687. https://doi.org/10.1109/JPROC.2010.2043032

Kottek, M., Grieser, J., Beck, C., Rudolf, B., & Rubel, F. (2006). World map of the Köppen-Geiger climate classification updated. *Meteorologische Zeitschrift*, *15*(3), 259–263. https://doi.org/10.1127/0941-2948/2006/0130

Kurtenbach, E., Eicker, A., Mayer-Gürr, T., Holschneider, M., Hayn, M., Fuhrmann, M., & Kusche, J. (2012). Improved daily GRACE gravity field solutions using a Kalman smoother. *Journal of Geodynamics*, *59–60*, 39–48. https://doi.org/10.1016/j.jog.2012.02.006

Kvas, A., Behzadpour, S., Ellmer, M., Klinger, B., Strasser, S., Zehentner, N., & Mayer-Gürr, T. (2019). ITSG-Grace2018: Overview and evaluation of a new GRACE-only gravity field time series. *Journal of Geophysical Research: Solid Earth*, *124*(8), 9332–9344. https://doi.org/10.1029/2019JB017415

Lambeck, K. (1988). *Geophysical geodesy: The slow deformations of the Earth*. Clarendon Press ; Oxford University Press.

Landerer, F. W., Flechtner, F. M., Save, H., Webb, F. H., Bandikova, T., Bertiger, W. I., et al. (2020). Extending the global mass change data record: GRACE follow-on instrument and science data performance. *Geophysical Research Letters*, *47*(12), e2020GL088306. https://doi.org/10.1029/2020GL088306

Lei, F., Crow, W., Shen, H., Parinussa, R., & Holmes, T. (2015). The impact of local acquisition time on the accuracy of microwave surface soil moisture retrievals over the contiguous United States. *Remote Sensing*, *7*(10), 13448–13465. https://doi.org/10.3390/rs71013448

Longuevergne, L., Wilson, C. R., Scanlon, B. R., & Crétaux, J. F. (2013). GRACE water storage estimates for the Middle East and other regions with significant reservoir and lake storage. *Hydrology and Earth System Sciences*, *17*(12), 4817–4830. https://doi.org/10.5194/hess-17-4817-2013

Mayer-Gürr, T., Behzadpour, S., Eicker, A., Ellmer, M., Koch, B., Krauss, S., et al. (2021). GROOPS: A software toolkit for gravity field recovery and GNSS processing. *Computers & Geosciences*, *155*, 104864. https://doi.org/10.1016/j.cageo.2021.104864

Mayer-Gürr, T., Behzadpur, S., Ellmer, M., Kvas, A., Klinger, B., Strasser, S., & Zehentner, N. (2018). ITSG-Grace2018 - Monthly, daily and static gravity field solutions from GRACE. *GFZ Data Services*. https://doi.org/10.5880/ICGEM.2018.003

Mekong River Commission. (2022). Mekong low flow and drought conditions in 2019-2021. Retrieved from https://www.mrcmekong.org/wp-content/uploads/2024/08/LowFlowReport20192021-1-1.pdf

Mishra, A. K., & Singh, V. P. (2010). A review of drought concepts. *Journal of Hydrology*, *391*(1–2), 202–216. https://doi.org/10.1016/j.jhydrol.2010.07.012

Naumann, G., Podesta, G., Marengo, J., Luterbacher, J., Bavera, D., Acosta Navarro, J., et al. (2023). Extreme and long-term drought in the La Plata Basin: event evolution and impact assessment until September 2022. (KJ-NA-31-381-EN-N (online)). https://doi.org/10.2760/62557

Nguyen, H., Wheeler, M. C., Hendon, H. H., Lim, E.-P., & Otkin, J. A. (2021). The 2019 flash droughts in subtropical eastern Australia and their association with large-scale climate drivers. *Weather and Climate Extremes*, *32*, 100321. https://doi.org/10.1016/j.wace.2021.100321

NOAA National Centers for Environmental Information. (2022). *ETOPO 2022 15 arc-second global relief model*. NOAA National Centers for Environmental Information. https://doi.org/10.25921/FD45-GT74

Oertel, M., Meza, F., Gironás, J., A. Scott, C., Rojas, F., & Pineda-Pablos, N. (2018). Drought propagation in semi-arid River Basins in Latin America: Lessons from Mexico to the Southern Cone. *Water*, *10*(11), 1564. https://doi.org/10.3390/w10111564

O'Neill, P. E., Peggy, E., Chan, S., Njoku, E., Jackson, T., Bindlish, R., & Chaubell, M. (2023). *SMAP L3 radiometer global daily 36 km EASE-grid soil moisture, version 9*. NASA National Snow and Ice Data Center Distributed Active Archive Center. https://doi.org/10.5067/4XXOGX0OOW1S

Owe, M., de Jeu, R., & Holmes, T. (2008). Multisensor historical climatology of satellite-derived global land surface moisture. *Journal of Geophysical Research*, *113*(F1), 687. https://doi.org/10.1029/2007JF000769

Owe, M., de Jeu, R., & Walker, J. (2001). A methodology for surface soil moisture and vegetation optical depth retrieval using the microwave polarization difference index. *IEEE Transactions on Geoscience and Remote Sensing*, *39*(8), 1643–1654. https://doi.org/10.1109/36.942542

Peltier, W. R., Argus, D. F., & Drummond, R. (2017). Comment on "An assessment of the ICE-6G_c (VM5a) glacial isostatic adjustment model" by Purcell et al. *Journal of Geophysical Research: Solid Earth*, *123*(2), 2019–2028. https://doi.org/10.1002/2016JB013844

Peters, E., Bier, G., Van Lanen, H., & Torfs, P. (2006). Propagation and spatial distribution of drought in a groundwater catchment. *Journal of Hydrology*, *321*(1–4), 257–275. https://doi.org/10.1016/j.jhydrol.2005.08.004

Preimesberger, W., Scanlon, T., Su, C.-H., Gruber, A., & Dorigo, W. (2021). Homogenization of structural breaks in the global ESA CCI soil moisture multisatellite climate data record. *IEEE Transactions on Geoscience and Remote Sensing*, *59*(4), 2845–2862. https://doi.org/10.1109/TGRS.2020.3012896

Rahmati, M., Amelung, W., Brogi, C., Dari, J., Flammini, A., Bogena, H., et al. (2024). Soil moisture memory: State-of-the-art and the way forward. *Reviews of Geophysics*, *62*(2), e2023RG000828. https://doi.org/10.1029/2023RG000828

Rasche, D., Blume, T., & Güntner, A. (2024). Depth extrapolation of field-scale soil moisture time series derived with cosmic-ray neutron sensing (CRNS) using the soil moisture analytical relationship (SMAR) model. *SOIL*, *10*(2), 655–677. https://doi.org/10.5194/soil-10-655-2024

Reichle, R., De Lannoy, G., Koster, R., Crow, W., Kimball, J., Liu, Q., & Bechtold, M. (2022). *SMAP L4 global 3-hourly 9 km EASE-grid surface and root zone soil moisture. Geophysical data, version 7*. NASA National Snow and Ice Data Center Distributed Active Archive Center. https://doi.org/10.5067/EVKPQZ4AFC4D

Reichle, R., Liu, Q., Ardizzone, J. V., Bechtold, M., Crow, W. T., De Lannoy, G., et al. (2023). Soil moisture active passive (SMAP) project assessment report for version 7 of the L4_sm data product. Retrieved from https://nsidc.org/sites/default/files/documents/technical-reference/smap_l4v7_sm_assessmtreport.pdf

Reynolds, C. A., Jackson, T. J., & Rawls, W. J. (2000). Estimating soil water-holding capacities by linking the food and agriculture organization soil map of the world with global pedon databases and continuous pedotransfer functions. *Water Resources Research*, *36*(12), 3653–3662. https://doi.org/10.1029/2000WR900130

Robinson, D. A., Campbell, C. S., Hopmans, J. W., Hornbuckle, B. K., Jones, S. B., Knight, R., et al. (2008). Soil moisture measurement for ecological and hydrological watershed-scale observatories: A review. *Vadose Zone Journal*, *7*(1), 358–389. https://doi.org/10.2136/vzj2007.0143

Rodell, M., Houser, P. R., Jambor, U., Gottschalck, J., Mitchell, K., Meng, C.-J., et al. (2004). The global land data assimilation system. *Bulletin of the American Meteorological Society*, *85*(3), 381–394. https://doi.org/10.1175/BAMS-85-3-381

Rossi, J. B., Ruhoff, A., Fleischmann, A. S., & Laipelt, L. (2023). Drought propagation in Brazilian biomes revealed by remote sensing. *Remote Sensing*, *15*(2), 454. https://doi.org/10.3390/rs15020454

Seneviratne, S. I., Zhang, X., Adnan, M., Badi, W., Dereczynski, C., Di Luca, A., et al. (Eds.), Climate change 2021: The physical science basis. Contribution of working group I to the sixth assessment report of the intergovernmental panel on climate change (pp. 1513–1766). Cambridge University Press. https://doi.org/10.1017/9781009157896.013

Sun, Y., Riva, R., & Ditmar, P. (2016). Optimizing estimates of annual variations and trends in geocenter motion and J2 from a combination of GRACE data and geophysical models. *Journal of Geophysical Research: Solid Earth*, *121*(11), 8352–8370. https://doi.org/10.1002/2016JB013073

Swenson, S., Chambers, D., & Wahr, J. (2008). Estimating geocenter variations from a combination of GRACE and ocean model output: Estimating geocenter variations. *Journal of Geophysical Research*, *113*(B8), B08410. https://doi.org/10.1029/2007JB005338

Tangdamrongsub, N., Han, S.-C., Yeo, I.-Y., Dong, J., Steele-Dunne, S. C., Willgoose, G., & Walker, J. P. (2020). Multivariate data assimilation of GRACE, SMOS, SMAP measurements for improved regional soil moisture and groundwater storage estimates. *Advances in Water Resources*, *135*, 103477. https://doi.org/10.1016/j.advwatres.2019.103477

Tapley, B. D., Bettadpur, S., Watkins, M., & Reigber, C. (2004). The gravity recovery and climate experiment: Mission overview and early results. *Geophysical Research Letters*, *31*(9), L09607. https://doi.org/10.1029/2004GL019920

Thomas, A. C., Reager, J. T., Famiglietti, J. S., & Rodell, M. (2014). A GRACE-based water storage deficit approach for hydrological drought characterization. *Geophysical Research Letters*, *41*(5), 1537–1545. https://doi.org/10.1002/2014GL059323

Tijdeman, E., Barker, L. J., Svoboda, M. D., & Stahl, K. (2018). Natural and human influences on the link between meteorological and hydrological drought indices for a large set of catchments in the contiguous United States. *Water Resources Research*, *54*(9), 6005–6023. https://doi.org/10.1029/2017WR022412

Ulaby, F. T., & Long, D. G. (2014). *Microwave radar and radiometric remote sensing*. The University of Michigan Press.

Van Loon, A. F. (2015). Hydrological drought explained. *WIREs Water*, *2*(4), 359–392. https://doi.org/10.1002/wat2.1085

Wagner, W. (1998). *Soil moisture retrieval from ERS scatterometer data (No. Heft 49)*. Wien: Veröffentlichung des Instituts für Photogrammetrie und Fernerkundung.

Wilhite, D. A., & Glantz, M. H. (1985). Understanding: The drought phenomenon: The role of definitions. *Water International*, *10*(3), 111–120. https://doi.org/10.1080/02508068508686328

Xiong, J., Guo, S., Abhishek, Li, J., & Yin, J. (2022). A novel standardized drought and flood potential index based on reconstructed daily GRACE data. *Journal of Hydrometeorology*, *23*(9), 1419–1438. https://doi.org/10.1175/JHM-D-22-0011.1

19447973, 2025, 8, Downloaded from https://agupubs.onlinelibrary.wiley.com/doi/10.1029/2024WR039321 by Hafencity Universitaet Hamburg, Wiley Online Library on [18/02/2026]. See the Terms and Conditions (https://onlinelibrary.wiley.com/terms-and-conditions) on Wiley Online Library for rules of use; OA articles are governed by the applicable Creative Commons License